



Parallel simulation of strong ground motions during recent and historical damaging earthquakes in Tokyo, Japan

T. Furumura ^{a,*}, L. Chen ^b

^a *Earthquake Research Institute, University of Tokyo, 1-1-1 Yayoi, Bunkyo-ku, Tokyo 113-0032, Japan*

^b *Research Organization for Information Sciences and Technology, 2-2-54 Nakameguro, Meguro-ku, Tokyo 153-0061, Japan*

Received 16 February 2004; revised 20 December 2004

Available online 14 April 2005

Abstract

The development of high-performance computing facilities such as the Earth Simulator supercomputer and the deployment of dense networks of strong ground motion instruments in Japan (K-NET and KiK-net) have made it possible to directly visualize regional seismic wave propagation during large earthquakes. Our group has developed an efficient parallel finite difference method (FDM) code for modeling the seismic wavefield and three-dimensional visualization techniques, both of which are suitable for implementation on the Earth Simulator. We will show examples of current state of the large-scale FDM simulations of seismic wave propagation by using the Earth Simulator to recast strong ground motions during damaging earthquakes in Tokyo such as the 2000 Tottori-ken Seibu ($M_{7.3}$) earthquake, the 1923 great Kanto earthquake ($M_{7.9}$), and the 1855 Ansei Edo (M_7) earthquake. Significant speed-up is achieved using 64–1406 processors of the Earth Simulator with good vector performance of over 40–60% of the theoretical peak speed.

© 2005 Elsevier B.V. All rights reserved.

* Corresponding author.

E-mail address: furumura@eri.u-tokyo.ac.jp (T. Furumura).

PACS: 02.70.Bf; 04.30.Nk; 91.30.-f; 91.30Mv

Keywords: Finite difference method; Parallel computing; Seismic wave; Strong ground motion

1. Introduction

The Tokyo metropolitan area is located in a very complicated tectonic region due to the simultaneous subduction of the Philippine Sea Plate and the Pacific Plate beneath the North American Plate. Large earthquakes frequently occur beneath Tokyo as a result of interactions among and within these plates. Thus, an important target for strong-motion seismologists is to understand the character of the seismic wavefield produced by such earthquakes and to predict the pattern of strong ground motions during future earthquake scenarios.

The seismic wavefield is strongly affected by heterogeneities in the crust and the upper mantle along the propagation path as well as complexities in source rupture processes on the fault plane over the plate. Small-scale heterogeneities such as sedimentary basins have the effect of amplifying ground motions by several times compared to surrounding bedrock sites, resulting in extended durations of large ground motion during an earthquake. For such scenarios, large-scale computer simulations using high-resolution structural models and complex source model are indispensable for achieving realistic simulations of seismic wave behavior.

The recent advancements in computing technology, such as the implementation of the Earth Simulator supercomputer (5120 processors, 40 TFLOPS), have made it possible to perform realistic simulations of seismic wave propagation on a regional scale. To exploit this computing power, our group has developed an efficient parallel finite difference method (FDM) code and concurrent volume visualization technique for the three-dimensional (3D) wavefield specifically for implementation on the Earth Simulator. The results of simulations using this technique can be compared with observations recorded by the new nation-wide seismic network (K-NET, KiK-net and FREESIA) comprising more than 1800 stations across Japan. Through detailed comparison between the simulations and observations, the accuracy of the simulation can be determined with respect to the main characteristics of strong ground motion during historical and future earthquake scenarios.

In this paper, the parallel FDM simulation for seismic waves is introduced, and an efficient visualization techniques [2] suitable for the Earth Simulator has been applied for the presentation of observed and simulated ground motions. The simulated seismic wavefield is first compared with the observation record for the recent 2000 Tottori-ken Seibu earthquake ($M_j7.3$) to verify the accuracy of the proposed FDM simulation. Simulations are then performed to reproduce ground motions during historical earthquakes such as the great 1923 Kanto earthquake ($M7.9$) and the 1855 Ansei Edo earthquake ($M7$), both of which caused significant damage in the Tokyo area.

2. Parallel simulation of seismic wave propagation

2.1. Equations of motions

Seismic wave propagation in elastic media is expressed by equations of motions in three dimensions as

$$\rho \ddot{u}_p = \frac{\partial \sigma_{xp}}{\partial x} + \frac{\partial \sigma_{yp}}{\partial y} + \frac{\partial \sigma_{zp}}{\partial z} + f_p \quad (p = x, y, z), \quad (1)$$

where σ_{pq} , f_p and ρ are the stress, body force and density, and \ddot{u}_p represents particle acceleration. The stresses in an isotropic elastic medium are given by

$$\sigma_{pq} = \lambda(e_{xx} + e_{yy} + e_{zz})\delta_{pq} + 2\mu e_{pq} \quad (p, q = x, y, z), \quad (2)$$

with Lamé's constants λ and μ . The strains are defined by

$$e_{pq} = \frac{1}{2} \left(\frac{\partial u_p}{\partial q} + \frac{\partial u_q}{\partial p} \right) \quad (p, q = x, y, z). \quad (3)$$

With the increment of time in Eq. (1), the velocity at the next time step $t = (n + 1/2)\Delta t$ is calculated by integration with respect to the time step Δt as follows.

$$\dot{u}_p^{n+1/2} = \dot{u}_p^{n-1/2} + \frac{1}{\rho} \left(\frac{\partial \sigma_{px}^n}{\partial x} + \frac{\partial \sigma_{py}^n}{\partial y} + \frac{\partial \sigma_{pz}^n}{\partial z} + f_p^n \right) \Delta t, \quad (4)$$

where $\dot{u}_p^{n+1/2}$ is the particle velocity at time $t = (n \pm \frac{1}{2})\Delta t$. Differentiation of Eqs. (2) and (3) with respect to time yields

$$\sigma_{pq}^{n+1} = \sigma_{pq}^n + \left[\lambda \left(\frac{\partial \dot{u}_x^{n+1/2}}{\partial x} + \frac{\partial \dot{u}_y^{n+1/2}}{\partial y} + \frac{\partial \dot{u}_z^{n+1/2}}{\partial z} \right) \delta_{pq} + \mu \left(\frac{\partial \dot{u}_p^{n+1/2}}{\partial q} + \frac{\partial \dot{u}_q^{n+1/2}}{\partial p} \right) \right] \Delta t \quad (p, q = x, y, z). \quad (5)$$

2.2. Boundary conditions

The boundary conditions for the displacement and stress components at the internal interfaces in the simulation model are implicitly treated in the FDM model by assigning suitable elastic parameters (λ, μ) and density (ρ) at each grid point. The free-surface boundary condition is simply incorporated into the calculation by introducing an air-filled zone with $\lambda = \mu = 0$ over the surface of the Earth. Artificial reflections at the physical boundaries outside of the 3D model are minimized by introducing an absorbing boundary condition based on the tapering approach [1], or more efficiently by adopting the Perfect Matching Layer [3].

2.3. Anelasticity

The anelastic (Q) attenuation in the medium for compressional (P) and shear (S) waves can be incorporated into the time-domain simulation either by applying

damping terms to the stress and velocity components at each grid point [9], or by introducing memory variables for the stress hysteresis curves [10]. The former model results in a strong frequency dependence in the attenuation characteristics of the seismic P and S wavefields ($Q(f) = Q_0 f^1$), whereas the latter model gives constant attenuation over a wide frequency range ($Q(f) = Q_0$).

2.4. Spatial derivatives

The spatial derivatives in Eqs. (4) and (5) can be calculated by the FDM, or more accurately by multiplying the wavenumbers in the wavenumber domain by using the fast Fourier transform (FFT) [7,15], which is called the Fourier Spectral Method (PSM).

The PSM has been recognized as a very efficient alternative to higher-order FDMs, as most FFTs run much faster than the higher-order FDMs of a large number of multiplications. For this reason, the PSM has long been used for large-scale 3D simulations of seismic wave propagation [7,15]. Fig. 1(a) compares the computation time for FDM and PSM modeling on a regular desktop computer (Intel Xeon 2.2 GHz) as a function of data size and the order of the FDM (4, 8, ..., 128). The experiment demonstrates that the PSM runs much faster than the higher-order FDMs for schemes of order higher than 32.

However, this does not apply to vector computers such as the Earth Simulator. By making full use of the vector hardware of the Earth Simulator, significant speed improvements can be achieved for the FDM simulation [Fig. 1(b)]. The benefits for FFT, on the other hand, are not as great for vector computing, even for special FFTs that are fully optimized for implementation on the Earth Simulator. A higher-order FDM was therefore selected for high-performance computation of seismic wave propagation instead of the PSM.

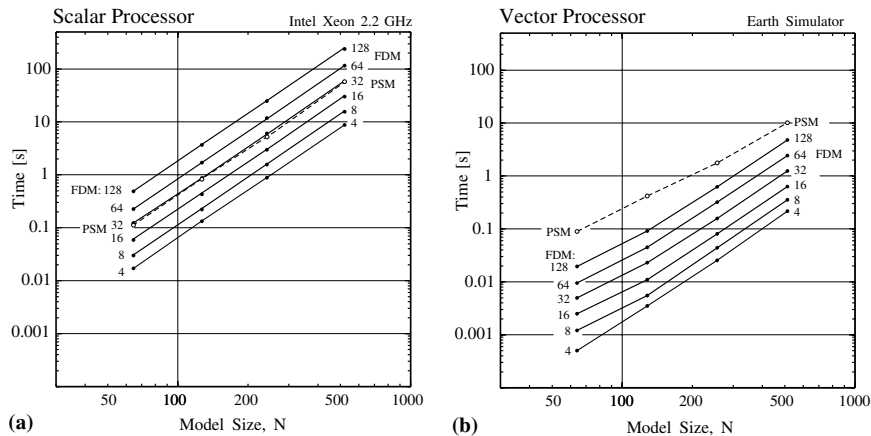


Fig. 1. Computation time for FDM (solid lines) and PSM modeling (dashed line) using (a) a scalar computer (Intel Xeon processor) and (b) a vector computer (Earth Simulator) as a function of data size and order of the FDM (4, 8, 16, ..., 128).

3. Parallel FDM simulation

Parallel simulation of a 3D seismic wavefield is achieved by a component decomposition approach [8] or domain partitioning procedure [4]. The former model decompose the equations of motion (Eqs. (4) and (5)) in three dimensions (x, y, z) into three sets of equations that can be assigned to three processors, thereby allowing for parallel computation using a few (three and its multiples) powerful computers.

Domain partitioning is more flexible with regard to the number of processors, and as such is suitable for massive parallel computing. Our domain partitioning model divides the 3D model vertically into many subregions that are assigned to many processors, and a message passing interface (MPI) is employed for the exchanged of data between neighboring node at each time step [Fig. 2(a)].

3.1. Parallel FDM simulation on the Earth Simulator

The Earth Simulator has a shared memory symmetric multiprocessor (SMP) cluster architecture and consists of 640 SMP nodes, where each SMP node is comprised of 8 vector processors. Dual-level parallel programming can therefore be applied for domain partitioning in the parallel FDM. A single-level flat MPI model is commonly used as a programming structure for the Earth Simulator, in which separate single-threaded MPI processes are executed on each processor [Fig. 2(b)]. An alternative approach that makes full use of the complex architecture of the Earth Simulator is multi-level parallelization using MPI between nodes in combination with loop-level parallelism within each node through compiler-based thread parallelization [e.g., Open MP; Fig. 2(c)]. Such an SMP/MPI hybrid approach requires somewhat complex programming, but does not incur a message-passing overhead for each

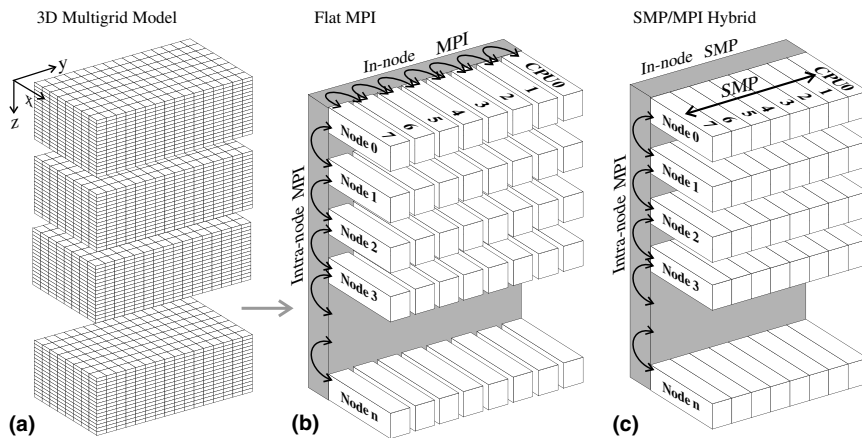


Fig. 2. (a) Schematic illustration of domain partitioning for 3D FDM simulation of seismic wave propagation, and (b,c) parallel computing procedure based on (b) a flat MPI parallel algorithm and (c) an SMP/MPI parallel algorithm.

SMP node. The efficiency of parallel computing using the flat MPI and SMP/MPI hybrid approaches has been discussed by many researchers [14].

Fig. 3 compares the performance of the parallel FDM simulation ($512 \times 512 \times 1024$ grid point model) for the two parallel algorithms mentioned above as a function of node number (4–64 nodes, 32–512 processors). Although both parallel models provide similar levels of performance for small numbers of nodes (processors), the SMP/MPI hybrid model displays somewhat better performance as the number of processors increases. The advantage of the hybrid parallel code is more clearly apparent in terms of the parallel work ratio, defined by the speed-up rate relative to the total number of processors [Fig. 3(b)]. The SMP/MPI hybrid approach extracts more performance from the domain-partitioned parallel FDM computing when using large numbers of processors, mainly because the flat MPI requires eight times as many MPI processes as the hybrid model, and so the necessary overhead of MPI data communication between the large number of subregions reducing the performance of the FDM simulation. Nevertheless, both parallel FDM approaches achieve good performance with efficiencies of 40–60% of the peak value for each processor (64 GFLOPS/node).

Fig. 4 illustrate the speed up of parallel FDM simulation as a function of the node number for a range of parallel computers. Good speed-up is achieved in parallel computing as the number of processor increases. These results also show that the Earth Simulator is 10 times faster than a HITACHI SR8000/MPP and 160 times faster than an Intel Xeon computer for FDM simulation using the same number of nodes. The parallel work ratio drops gradually with increasing node number above 16, due mainly in this case to over-partitioning of the small grid model ($256 \times 512 \times 384$), where the large number of processors results in very short vector lengths in the partitioned (z) direction.

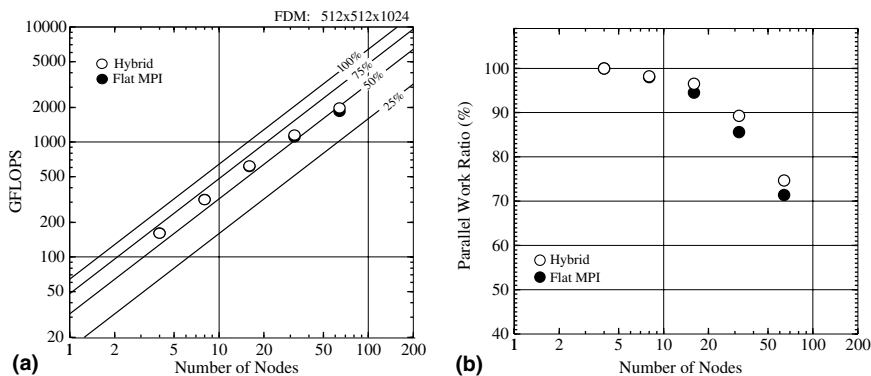


Fig. 3. Parallel performance of the Earth Simulator for 3D parallel FDM simulation using 4–64 nodes using flat MPI and SMP/MPI. (a) Performance in GFLOPS and the efficiency (25%, . . . , 100%) relative to peak performance, and (b) parallel work ratio relative to peak performance.

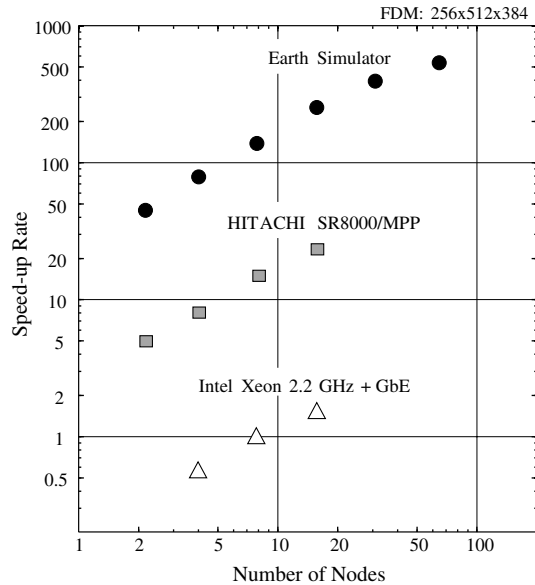


Fig. 4. Speed-up of parallel FDM simulation using the Earth Simulator, a Hitachi SR8000/MPP, and a cluster of Intel Xeon computers as a function of processor number (nodes).

4. Visualization of 3D seismic wavefield

Visualization of the 3D seismic wavefield is very important for extracting the salient features of a seismic wavefield from the large data set obtained by large-scale simulation. As supporting visualization tools for the parallel FDM simulation, our group also developed a set of efficient visualization techniques for presenting simulated and observed seismic wavefields in a manner that facilitates understanding of the complex seismic behavior in 3D heterogeneous structures.

4.1. Bird's eye view of surface ground motion

One of the visualization techniques used in the present application renders a 2D seismic wavefield, which is suitable for visualizing phenomena such as surface ground motions. This approach for visualization of the wavefront is useful for illustrating the propagation of ground motion derived from simulations and observations recorded by a dense seismic array [6]. In this technique, the ground motion is first passed through a high-cut filter to eliminate aliasing. Smoothed ground motion is then obtained as gridded data by interpolation of the filtered waveform using a gridding algorithm developed by Smith and Wessel [16]. As the intensity of ground motion manifests on a logarithmic scale of horizontal ground velocity motion, the logarithmic scalar value of the strength of the ground motion is a useful representation of the strength of ground motions. The resulting scalar at each point on the regular mesh, for both observed and simulated ground motions, is then used to render the wavefront

using the height-field function of the POV-Ray rendering library. To highlight the wavefront of larger ground motions and eliminate weak and scattered wavefields (e.g., less than 0.1% of the peak ground motion), an opacity function proportional to the logarithmic amplitude of the ground motion is applied for rendering.

4.2. Concurrent parallel volume rendering of seismic wavefield

Another visualization technique used here is volume visualization of the simulated 3D seismic wavefield based on the volume rendering technique [12]. As the 3D simulation produces huge data sets in each time step, it is difficult to store all of the simulation results on an external hard disk for post processing. Our group therefore developed a concurrent parallel volume rendering (PVR) tool for visualization of the 3D wavefield suitable for implementation on the Earth Simulator [2]. This concurrent technique utilizes data stored in the main memory of the computer, eliminating the need to store huge amounts of data to external media or other machines over the network. During the parallel calculations for seismic waves, the main program of the FDM simulation on each node calls the PVR module at each time step to generate a frame image from the simulated wavefield at the current time using the variables held in the memory. The large dynamic range of the seismic wavefield amplitude is compressed using a logarithm function, by which a low opacity (large transparency) is assigned to grid points of weak wavefield amplitude and relatively high opacity is assigned to strong wavefield points. This has the effect of highlighting the outline of the seismic wavefield clearly and prevents small, scattered waves from obscuring important features [4]. The quality of volume rendering can be improved by choosing appropriate opacity transfer functions. In this case, transfer functions that emphasize the high-gradient seismic regions were selected.

As the graphics processing ability of the Earth Simulator is rather limited, without graphics hardware capable of texture mapping or alpha-blending etc., the PVR module makes full use of the vector hardware and SMP/MPI hybrid parallel computing to obtain good visualization performance. The current PVR module is, however, still very slow compared with the parallel FDM simulation itself. For example the computation time for volume visualization of a $512 \times 256 \times 512$ model with an image resolution of 640×480 is about 1 s by parallel computing using 16 nodes (256 processors), which is about ten times slower than the FDM simulation (about 0.1 s per time step). Thus, improving the performance of volume visualization on the Earth Simulator remains an important subject of our current study.

5. Parallel simulation of the 2000 Tottori-ken Seibu earthquake

The 200 Tottori-ken Seibu earthquake was a large ($M_J7.3$) inland earthquake that occurred in Tottori, Japan. This was the largest event since the destructive Kobe earthquake ($M_J7.2$) in 1995. The ground motion from the large earthquake was recorded at 521 stations of the nation-wide dense strong-motion network (K-NET and KiK-net; Fig. 5), which was deployed following the Kobe earthquake in order to

mitigate future earthquake disasters by developing an understanding of wave propagation and localized amplification characteristics during large earthquakes.

Seismic wave propagation associated with the Tottori-ken Seibu earthquake was simulated in order to demonstrate the accuracy of the proposed large-scale parallel simulation by comparison with the ground motions recorded by the dense seismic array. The simulation modeled an area of 820 km by 410 km area and extended to a depth of 128 km, which was discretized into elements with dimensions of 0.8 km by 0.8 km in the horizontal direction and 0.4 km in the vertical direction. The model was surrounded by a 20-gridpoint absorbing buffer zone [1] to eliminate artificial reflections.

The subsurface structure model of western Japan was constructed based on a large number of datasets obtained by reflection and refraction surveys and travel-time tomography studies. The 3D model included lateral changes in the crust/mantle interface and the depth of the Philippine Sea Plate [Fig. 6(a)]. The fault rupture history for the earthquake was derived by inversion using the K-NET and KiK-net records and teleseismic waveforms [18]. The source model was defined as a set of point double-couple sources on the fault plane, each radiating seismic waves with a maximum frequency of 1 Hz.

The 3D model was partitioned vertically into 32 subdomains of equal grid numbers, and each subdomain was assigned to the same number of nodes of the Earth Simulator. The parallel simulation used 100 Gbyte of memory and took a wall-clock time

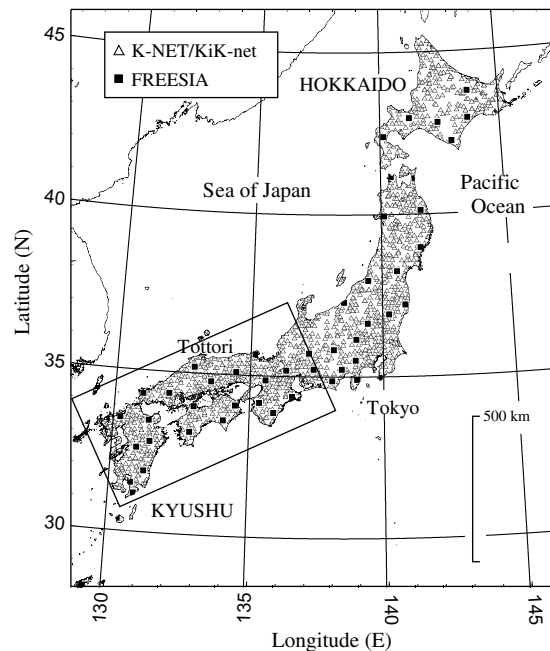


Fig. 5. Coverage of strong ground motion instruments (K-NET, KiK-net; triangles) and FREESIA broadband stations (squares) across Japan, incorporating over 1800 stations. Rectangle denotes the area of computer simulation.

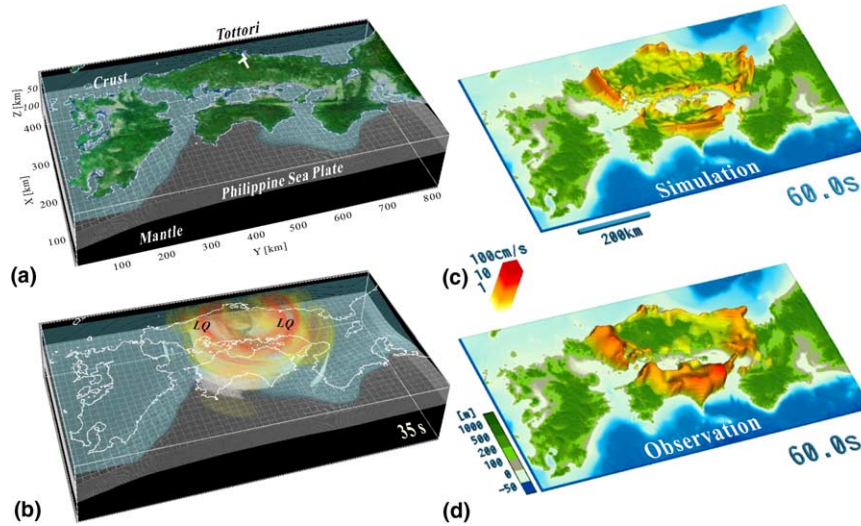


Fig. 6. (a) Structural model of western Japan used in the 3D simulation of seismic waves, showing the configuration of crust and upper mantle and the Philippine Sea Plate. (b) Snapshot of seismic wave propagation from the source 35 s after source initiation, and (c, d) comparison of the (c) simulated and (b) observed wavefield at 60 s.

of about 20 min for parallel computation using 32 nodes (256 processors). The parameters for the 3D simulation of the Tottori-ken Seibu earthquake are listed in Table 1.

Fig. 6 shows a set of snapshots of the simulated seismic wavefield. The shallow source of the earthquake radiated large S waves in the crust, which can be clearly seen in the first frame of the 3D wavefield [Fig. 6(b)] as a four-lobe pattern of large S waves surrounding the source. As time increases, the development of large-amplitude surface waves (LQ) on the surface can also be clearly seen. The LQ waves propagate in western Japan at a relatively low wave speed of about 2.7 km/s, corresponding to a period of over 1 min to propagate out from the source to Kyushu.

The ground motions observed on a regional scale by the dense seismic array clearly confirm the accuracy of the computer simulation. The effect of deep basin

Table 1
Parameters for 3D simulation of the 2000 Tottori-ken Seibu earthquake

Model name	Tottori
Model size	820 km \times 410 km \times 128 km
Resolution	0.8 km \times 0.8 km \times 0.4 km
Number of grid points	168 million
Total time steps	6000
Memory	43 Gbyte
Number of nodes (processors)	32 (256)
Computation time	20 min
Performance	1228 GFLOPS

structures in major population centers can also be clearly seen as regions of significant amplification and extension of ground oscillations. The correlation between the observations [Fig. 6(c)] and the simulation [Fig. 6(d)] is very good, except for a slight underestimation of the amplitude of surface waves. This minor discrepancy is due to an incomplete simulation of the amplification effect in the shallow layer because of the large grid size (0.4 km) employed in the present model. Nevertheless, the good match between the simulation and observations demonstrates that the model can be used with good reliability to reproduce the patterns of ground motions associated with historical damaging earthquakes and future earthquakes.

6. Ground motion during the 1923 Kanto earthquake

The parallel FDM simulation was employed to reproduce ground motions associated with the historical damaging earthquake that struck the Tokyo metropolitan area in 1923. The great 1923 Kanto earthquake ($M7.9$) was one of the most destructive earthquakes in recent Japanese history, with over 100,000 casualties in the Tokyo and Yokohama area. Most of the damage was attributed to the subsequent firestorm fueled by wooden-framed houses. The Kanto earthquake occurred at the interface of the subducting Philippine Sea plate beneath the Kanto area. The Tokyo metropolitan area is located on a large Kanto basin with thick sediments overlying rigid bedrock, resulting in significant amplification of ground motion and very long shaking times of several minutes on the surface.

Historical documentation suggests that this type of earthquake has occurred repeatedly in Tokyo, with a regular recurrent interval of about 200 years. Thus, developing a comprehensive understanding of the fault rupture process and strong ground motions during the 1923 event will aid the design of emergence preparedness for the next potentially damaging earthquake.

The strong ground motion during the earthquake was recorded by early seismic instrumentation in Tokyo, but unfortunately most of the records are clipped (saturated) at large amplitudes of >30 mm over a long shaking time. The present simulation was therefore conducted in order to reconstruct the strong ground motions that struck Tokyo in 1923.

The simulation model is shown in Table 2. The model covers a zone that includes the Kanto basin, which is comprised of heterogeneous crust and upper mantle overlying the subducting Philippine Sea Plate. Appropriate elastic parameters and anelastic attenuation coefficients for P and S waves were assigned at each grid point, as derived from a number of geophysical experiments [19]. The subsurface structural model of the Kanto basin was defined to consist of three sedimentary layers with a minimum S-wave velocity of 0.5 km/s, 1.0 km/s and 1.7 km/s, respectively, overlying rigid bedrock with an S-wave velocity of 3.2 km/s. The maximum thickness of the sedimentary layer was about 4 km, located at the center of Tokyo bay [Fig. 7(a)].

The seismic source model was derived from an analysis of teleseismic waveforms [17], and is represented by two large slips (>6 m) on the fault area of about

Table 2
Parameters for 3D simulation of the 1923 Kanto earthquake

Model name	Kanto
Model size	204 km × 204 km × 100 km
Resolution	0.2 km × 0.2 km × 0.1 km
Number of grid points	1040 million
Total time steps	16,000
Memory	260 Gbyte
Number of nodes (processors)	64 (512)
Computation time	60 min
Performance	2406 GFLOPS

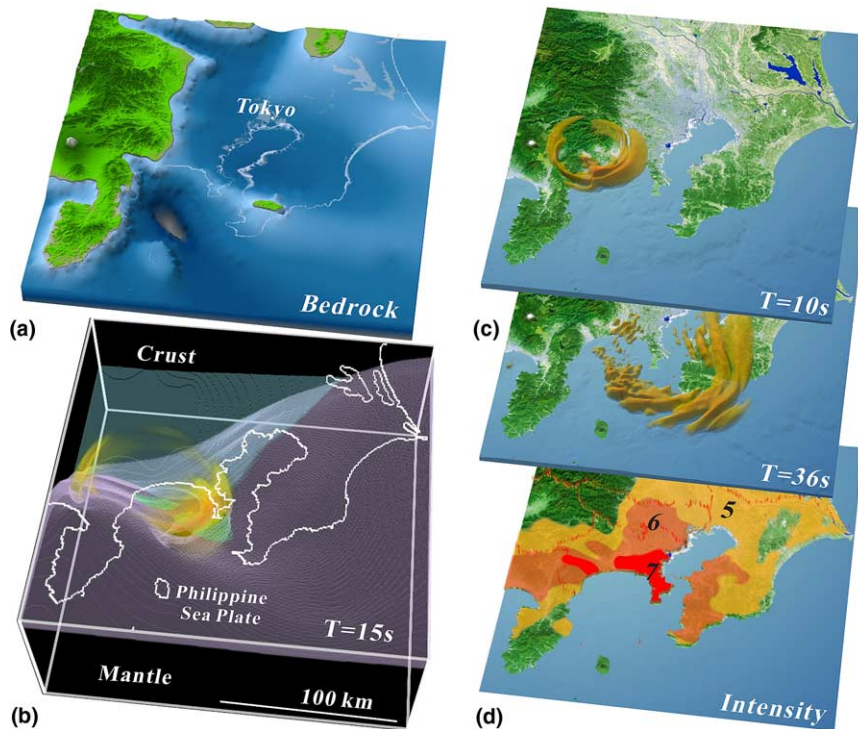


Fig. 7. (a) Structural model of sediment/bedrock interface beneath Tokyo. (b,c) Snapshot of seismic wave propagation (b) radiating from the source (green area) on the Philippine Sea Plate during the 1923 Kanto Earthquake, and (c) for two large pulses on the surface. (d) Simulated intensity of ground motion associated with the Kanto earthquake.

30 × 120 km. The fault rupture initiated beneath the Miura peninsula and propagated to the southeast at a speed of about 2.5 km/s [17].

The simulation results are shown in Fig. 7 as snapshots of seismic wave propagation. These snapshots show the generation of strong ground motion by rupture propagation on the subducting Philippine Sea Plate and amplification in the

heterogeneous structure of Kanto basin. Two large seismic pulses with wavelengths of the order of kilometers can be seen to propagate in Tokyo at a relatively low propagation speed of less than 2 km/s and with a dominant frequency of 0.2–0.5 Hz. Such low-frequency ground motions of relatively long wavelength can propagate longer distances from the source, reaching the center of Tokyo with less attenuation than high-frequency seismic signals. The soft sediments of more than 4 km in thickness covering the basin amplified the long-period seismic wave significantly by resonance in the low wavespeed layer. The visualized seismic wavefield indicates that the ground motion damage occurred as a result of a complex mechanism related to the complex fault rupture process at the source and dramatic amplification in the heterogeneous structure along the propagation path and the shallow structure of the Tokyo basin.

The estimated seismic intensity on the Japanese 7-point scale is shown in Fig. 7(d). Large ground motions with an intensity of greater than 6 can be seen over a wide area above the hypocenter. The pattern of seismic intensity agrees well with the damage rates of wooden-framed houses [13].

7. Source depth estimation for the 1855 Ansei Edo earthquake

Simulation of seismic wave propagation and the resultant intensity pattern is an important tool for estimating the source model of historical damaging earthquakes. The Tokyo metropolitan area is known to have been struck with three large earthquakes with seismic intensity of greater than 6; the 1923 Kanto earthquake ($M7.9$), the 1703 Genroku earthquake ($M8.4$), and the 1855 Ansei Edo earthquake ($M7$). Whereas the former two events are known to have occurred at the top of the subducting Philippine Sea Plate, the latter is considered to have occurred in Tokyo bay but at an unknown source depth.

Many researchers have attempted to determine the source mechanism of the 1855 Ansei Edo earthquake through analysis of the pattern of seismic intensity distribution in Tokyo. However, the intensity pattern in the center of Tokyo would be considerably affected by the site amplification effects of the shallow, localized structure rather than be related directly to the source itself, and thus it has proved very difficult to estimate the source depth from the local intensity pattern in Tokyo (e.g. [11]).

In the present analysis, the intensity distribution on a regional scale was employed because the major features of the seismic intensity pattern on regional scales would be affected by deep and large-scale subsurface structures in the crust and upper mantle rather than small-scale heterogeneities in the shallow structure beneath Tokyo. In the intensity pattern for the 1855 Ansei Edo earthquake [Fig. 8(a)], a peculiar distribution of intensity can be seen on a regional scale, with a rapid decay in intensity from 6 to 5 over the hypocenter but a broad extension of the intensity 4 region over an area of several hundred kilometers in central Japan. The intensity displays an almost isoseismal pattern above the hypocenter, with no clear extension of intensity contours to the north as usually seen during deep earthquakes occurring on the subducting Pacific Plate.

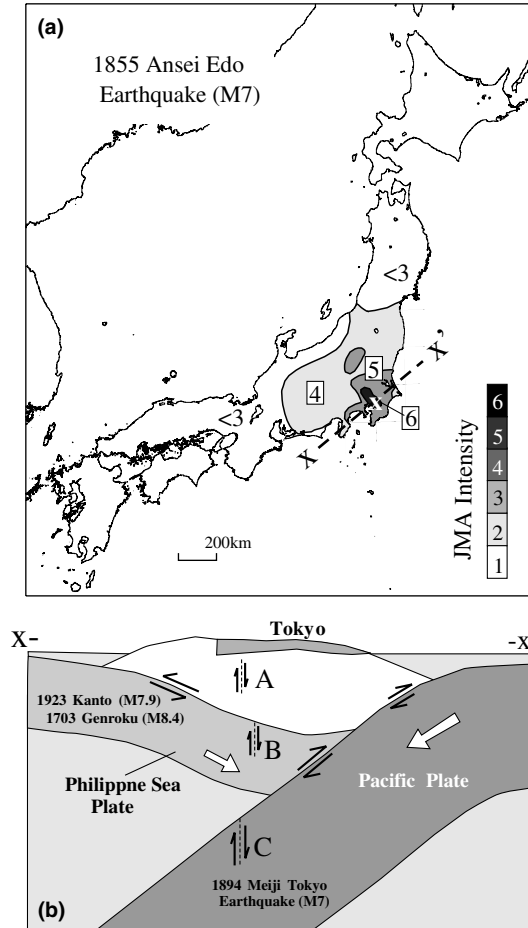


Fig. 8. (a) Pattern of seismic intensity during the 1855 Ansei Edo earthquake. (b) Schematic illustration of vertical cross section through Tokyo $x-x'$ and mechanism of major earthquakes below Tokyo. Rectangle denotes the area of the simulation.

The effect of source depth on the regional seismic wavefield was examined by conducting a series of simulations using three possible source models; (A) a crustal source ($h = 8$ km), (B) a source on the Philippine Sea Plate (35 km), and (C) a source on the Pacific Plate (80 km). The large-scale parallel FDM simulation allows seismic wave propagation to be simulated on a regional scale for frequencies of over 3 Hz, where the intensity of ground motions is strongly dependent on higher-frequencies around 1–2 Hz. The parameters for the high-frequency regional simulation are listed in Table 3.

Fig. 9(b) shows snapshots of seismic wave propagation following a deep ($h = 80$ km) event occurring on the Pacific Plate. Large-amplitude P and S waves can be seen to propagate in northern Japan. As the subduction of the Pacific Plate

is capable of transmitting high-frequency seismic signals for longer distances without attenuation compared to propagation in the surrounding mantle, the resultant inten-

Table 3
Parameters for 3D simulation of the 1855 Ansei Edo earthquake

Model name	Tohoku
Model size	820 km × 410 km × 400 km
Resolution	0.4 km × 0.4 km × 0.2 km
Number of grid points	4 billion
Total time steps	16,000
Memory	1 Tbyte
Number of node (CPU)	176 (1024)
Computation time	120 min
Performance	6758 GFLOPS

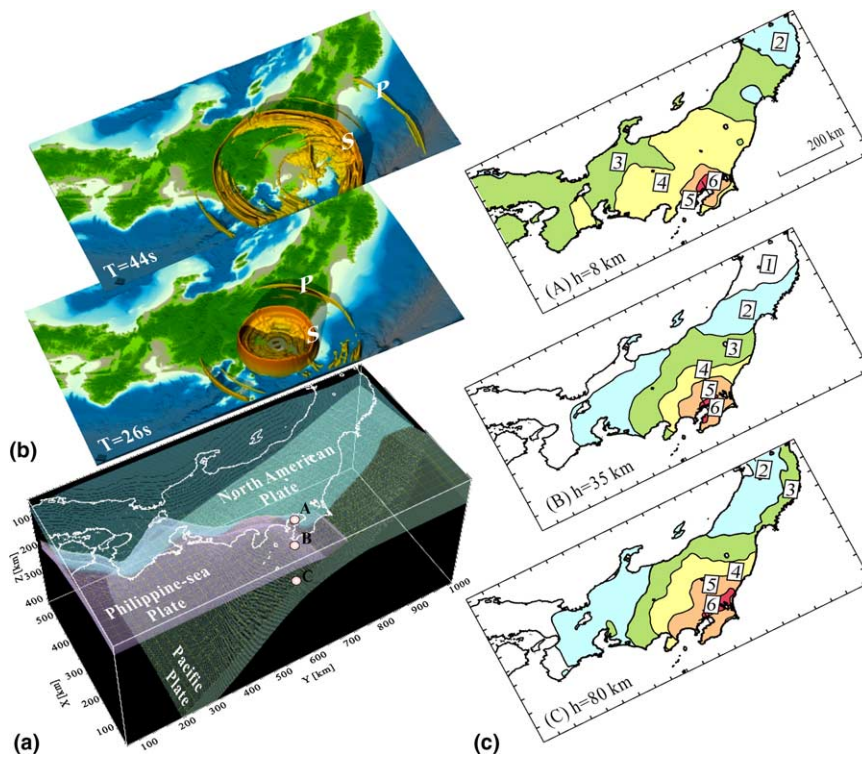


Fig. 9. (a) Structural model of central Japan used in the 3D simulation of seismic wave propagation, showing the configuration of the crust and upper mantle, the Philippine Sea Plate, and the Pacific Plate. (b) Snapshots of seismic wave propagation on the surface associated with a deep Pacific Plate event ((C) in panel(a)) 26 s and 44 s after source initiation, and (c) simulated intensity pattern for three events at source depths of (A) 8 km, (B) 35 km, and (C) 80 km.

sity distribution includes anomalously high values along the eastern seaboard of northern Japan [Fig. 9(c-(C))].

The simulated intensity for the intermediate depth ($h = 35$ km) earthquake in the Philippine Sea Plate exhibits an almost isoseismal contour distribution above the hypocenter, with only slight extension of the contours along the plate. This resembles the pattern of intensity during the 1923 Kanto earthquake.

The shallow ($h = 8$ km) source produces a completely different intensity pattern compared to the other two earthquakes scenarios, with an almost isoseismal pattern above the hypocenter and no directional elongation. The intensity decays very quickly from 6 to 5 above the hypocenter, and then weakens with a more gentle gradient from 4 to 3, with attenuation extending over several hindered kilometers from the hypocenter [Fig. 9(c-(A))].

By comparison with observations, the preferable source model for the 1855 Ansei Edo earthquake is the shallow ($h = 8$ km) event as a crustal source. The snapshots of the seismic wavefield and the simulated waveform reveals that the weaker decay of seismic intensity is due to the dominance of multiple S-wave reflections in the crust, known as the *Lg* wave. Such a crustally trapped *Lg* wave is often recognized in regional seismographs in Japan at distances of over 150 km from the epicenter as the largest S waves during shallow crustal earthquakes [5].

8. Conclusions

Complex source rupture histories and heterogeneities of the subsurface structure along the wave propagation path can result in highly complex seismic wavefields. The prediction of strong motion during future events therefore requires a good understanding of the seismic wavefield resulting from such heterogeneities. Our predictive ability is steadily increasing through the combination of dense seismic observation networks and high-resolution computer simulations and the development of better 3D visualization techniques. Recent advancements in high-performance parallel computing facilities such as the Earth Simulator and dense nation-wide seismic networks (K-NET and KiK-net) have made it possible to perform such collaborative studies.

In the present study, simulations of recent and historical damaging earthquakes were demonstrated to achieve a suitable level of accuracy for the reproduction of seismic wave propagation and pattern of intensity, allowing for the prediction of strong ground motion patterns during large earthquakes. Further improvements in the understanding of complex seismic wavefields and highly reliable computer simulations will depend on maintaining close link between seismology and computer sciences.

Acknowledgments

This study was supported under a joint research project in cooperation with the Earth Simulator Center entitled “Numerical simulation of seismic wave propagation and strong ground motion in 3D heterogeneous media”. Figures were prepared

using the POV-Ray rendering software developed by C. Cason. This study was also supported under the Special Project for Earthquake Disaster Mitigation in Urban Areas of the Ministry of Education, Culture, Sports, Science and Technology of Japan. K-NET and KiK-net waveform data are available on the NIED website (<http://www.bosai.go.jp>). Critical review and comments from two anonymous reviewers are greatly appreciated.

References

- [1] C. Cerjan, K. Kosloff, R. Kosloff, M. Reshef, A nonreflecting boundary condition for discrete acoustic and elastic wave equation, *Geophysics* 50 (1985) 705–708.
- [2] L. Chen, I. Fujisihoro, K. Nakajima, Optimizing parallel performance of unstructured volume rendering for the Earth Simulator, *Parallel Comput.* 29 (2003) 355–371.
- [3] F. Collino, C. Tsogka, Application of the perfectly matched absorbing layer model to the linear elastodynamic problem in anisotropic heterogeneous media, *Geophysics* 66 (2001) 294–307.
- [4] T. Furumura, L. Chen, Large scale parallel simulation and visualization of 3D seismic wavefield using the Earth Simulator, *Comput. Model. Eng. Sci.* 6 (2004) 153–168.
- [5] T. Furumura, B. Kennett, Variations in regional phase propagation in the area around Japan, *Bull. Seismol. Soc. Am.* 91 (2001) 294–308.
- [6] T. Furumura, B. Kennett, K. Koketsu, Visualization of 3D wave propagation from the 2000 Tottori-ken Seibu, Japan Earthquake: observation and numerical simulation, *Bull. Seismol. Soc. Am.* 93 (2003) 870–881.
- [7] T. Furumura, B. Kennett, H. Takenaka, Parallel 3-D pseudospectral simulation of seismic wave propagation, *Geophysics* 63 (1998) 279–288.
- [8] T. Furumura, K. Koketsu, Parallel 3D simulation of ground motion for the 1885 Kobe earthquake: the component decomposition approach, *Pure Appl. Geophys.* 157 (2000) 2047–2062.
- [9] R. Graves, Simulating seismic wave propagation in 3-D elastic media using staggered-grid finite differences, *Bull. Seismol. Soc. Am.* 86 (1996) 1091–1106.
- [10] S. Hestholm, Three-dimensional finite difference viscoelastic wave modelling including surface topography, *Geophys. J. Int.* 139 (1999) 852–878.
- [11] T. Hikita, K. Kudo, Estimation of source parameters and strong ground motions during the 1855 Ansei-Edo earthquake by the empirical Green function method, *J. Struct. Eng. AIJ* (2001) 63–70.
- [12] M. Levoy, Display of surfaces from volume data, *IEEE CG&A* 8 (1988) 29–37.
- [13] T. Moroi, M. Takemura, Re-evaluation on the damages statistics of wooden houses for the 1923 Kanto earthquake and its seismic intensity distribution in and around Southern Kanto district, *J. Seismol. Eng. Japan* (2002) 35–71.
- [14] K. Nakajima, Parallel iterative linear solvers with preconditioning for large scale problems, Ph.D. thesis, Tokyo University, 2002.
- [15] M. Reshef, D. Kosloff, M. Edwards, C. Hsiung, Three dimensional acoustic modeling by the Fourier method, *Geophysics* 53 (1988) 1175–1183.
- [16] W. Smith, P. Wessel, Gridding with continuous curvature splines in tension, *Geophysics* 55 (1990) 293–305.
- [17] D. Wald, P. Somerville, Variable-slip rupture model of the great 1923 Kanto, Japan, earthquake: geodetic and body-waveform analysis, *Bull. Seismol. Soc. Am.* 85 (1995) 159–177.
- [18] Y. Yagi, M. Kikuchi, Source rupture process of the Tottori-ken Seibu earthquake of October 6, 2000, (Mjma 7.3) by using joint inversion of far-field and near-field waveform, *Abst. Seism. Soc. Japan 2000 Fall Meeting*, T04.
- [19] H. Yamanaka, N. Yamada, Estimation of 3D S-wave velocity model of deep sedimentary layers in Kanto plain, Japan, using microtremor array measurements, *Butsuri-Tansa* 55 (2002) 53–65.